RANS MODELING OF FLOW IN ROTATING CAVITY SYSTEM

Sébastien Poncet, Riccardo da Soghe, Bruno Facchini

V European Conference on Computational Fluid Dynamics
ECCOMAS CFD 2010
J. C. F. Pereira and A. Sequeira (Eds)
Lisbon, Portugal,14-17 June 2010

RANS MODELING OF FLOW IN ROTATING CAVITY SYSTEM

S. Poncet*, R. Da Soghe, and B. Facchini††

* Laboratoire M2P2, UMR 6181 CNRS - Aix-Marseille University
Technopôle Château-Gombert, 38 rue F. Joliot-Curie, 13451 Marseilles (France)
e-mail: poncet@L3m.univ-mrs.fr
††Energy Engineering Department "S. Stecco", University of Florence
50139, via S. Marta 3, Florence (Italy)
e-mail: riccardo.dasoghe@htc.de.unifi.it

Key words: Rotating cavity, rotor-stator, Taylor-Couette-Poiseuille flow, Reynolds Stress Model, CFD

Abstract. *The accurate prediction of fluid flow within rotating systems has a primary role for the reliability and performance of gas turbine engine. The selection of a suitable turbulence model for the study of such complex flows remains an open issue in the literature. This paper reports a numerical benchmark of the most used eddy viscosity RANS models available within the commercial CFD solvers Fluent and CFX together with an innovative Reynolds Stress Model closure. The predictions are compared to experimental data and previous numerical calculations available in the open literature for three test cases. Test case 1 corresponds to a rotating cavity with a radial outflow, considered experimentally by Owen and Pincombe [19]. In that case, the main difficulty arises from the choice of the boundary conditions at the outlet. Several types of boundary conditions have been then considered. All models fail to predict the radial velocity distribution. Nevertheless, the RSM offers the best agreement against the experimental data in terms of the averaged tangential velocity in the core. Test case 2 corresponds to a Taylor-Couette system with an axial Poiseuille flow studied experimentally by Escudier and Gouldson [6]. Even if the two-equation models provide reliable data for the mean velocity field, they strongly underestimate the turbulence intensities everywhere. The agreement between the RSM and the measurements is rather satisfactory for the mean and turbulent fields, though this second-order closure does not predict the asymmetry of the normal stresses. The main discrepancies appear indeed very close to the stator. Test case 3 is a rotor-stator system with throughflow, corresponding to the test rig of Poncet et al. [22, 23]. All the models catch the main features of rotor-stator flows, such as the value of the entrainment coefficient or the location of the transition from the Stewartson to the Batchelor flow structures. The RSM improves especially the predictions of the shear stress.*

INTRODUCTION

Rotating flows have been widely considered during the last decades mainly because of their relevance in many industrial applications. We can cite among others, magnetic storage devices, semi-conductor manufacturing processes with rotating wafers, generator rotors or gas turbine engines. In these configurations, the flows present several complexities (three-dimensionality, wall effects, imposed throughflow, transitional zones, relative motion between elements, anisotropic turbulence, high rotation rate ...), which are very challenging for numerical approaches. Up to now, the most frequently adopted turbulence closures in such applications invoke the linear eddy-viscosity hypothesis for the mean flow and scalar transport equations for turbulence. Among the two-equation eddy-viscosity based turbulence model, $k-\epsilon$ model is widely used in case of very complex geometries without excessive computational costs. On the other hand, like the other one-point first-order turbulence models in their original form, it is not sensitized to system rotation effects on turbulence. There are two types of effects, which are crucial to mimic in the context of rotating machinery applications: direct effects due to the Coriolis force on the generation of turbulent energy and indirect effects caused by the restructuration of the flow field by the mean velocity.

One way to sensitize turbulence models to rotation effects is to modify the turbulent length scale by adding rotation dependent terms to the dissipation rate equation. Thus, Howard et *al*. [10] considered turbulent flows in rotating ducts using a modified $k-\epsilon$ model, whose coefficients depend on the rotation rate. Hellsten [9] introduced another correction corresponding to a curvature correction in a $k-\omega$ SST model. Following the early work of Howard et *al*. [10], Cazalbou et *al*. [2] proposed a linear $k-\epsilon$ model, which accounts for the inhibition of the cascade to small scales and for the shear/Coriolis instability. It has been validated in two test cases (initially isotropic turbulence and homogeneously sheared turbulence), where the Coriolis accelerations directly influence the fluctuating field without affecting the mean flow. A different approach is based on the work of Gatski and Speziale [8], who derived an explicit solution to the algebraic stress representation of a linear second-moment closure in a non inertial frame. Iaccarino et *al*. [11] modified the former $\overline{v^2}-f$ model by introducing a dependence of the coefficient c_μ (contained in the definition of the eddy viscosity) on the invariants. They validated their model in three test cases where turbulence dominates the overall effect of imposed system rotation: a rotating channel flow, a rotating backstep, and a rotating cavity with an impinging jet.

Within the second-moment closures, system rotation appears in the Reynolds stress transport equations by interaction with anisotropy in the intercomponent transfer terms. Some implicit effects of rotation need all the same to be taken into account. For example, Coriolis accelerations modify the fluctuating field by an inhibition of the energy cascade to small scales. Elena and Schiestel [5] proposed a RSM model in its third version, where additional terms in the stress transport equations act only when the flow is subjected

to strong rotation. It includes a dependence of the pressure-strain correlation to the Reynolds and Cambon structure tensor, a spectral jamming term enhancing bidimensionality and the blocking effect of the spectral transfer. These modifications improved the predictions in rotor-stator flows with a better prediction of the location of the relaminarized and turbulent regions and of the turbulence levels close to the rotor.

The selection of a suitable turbulence model for the study of rotating flows remains an open issue in the literature. Previous works showed that the flow in rotating disk systems with throughflow can be computed with reasonable accuracy using $k-\epsilon$ models (see [26]). Even if second-moment closures are not always tractable in complex applications due to excessive computational cost, the purpose of the present work is to perform a benchmark of some turbulence models in three different rotating flow arrangements with throughflow and to propose the turbulence model offering the best trade-off between accuracy and computational cost for each configuration.

NUMERICAL MODELING

In the next section, a brief description of some of the two-equation turbulence models available within the commercial codes Fluent and CFX is given. Then, the RSM model of Elena and Schiestel [5] sensitized to rotation effects is presented.

Two-Equations Turbulence Models

The standard k-ε, k-ω and k-ω SST models in their formulation kept available by the commercial CFD 3D solvers Fluent 6.3 and CFX-12.0 have been selected for all calculations presented here. All models were used in their original form, i.e. no tuning of the turbulence model constants was done.

The k-ε turbulence model solves two transport equations, one for the turbulence kinetic energy k and the other one for its dissipation rate ε. As usual for the two equations model, the transport equation for k is derived from the exact equation, while the equation for its dissipation rate is obtained using physical reasoning. In its original form, the k-ε model is not sensitized to rotation and curvature effects.

The k-ω SST turbulence model solves two transport equations, one for the turbulence kinetic energy k and one for the specific dissipation ω. The idea of the SST model is to retain the robust and accurate formulation of the Wilcox k-ω model in the near wall region [16], and to take advantage of the free stream independence of the k-ε model in the outer part of the boundary layer. To achieve this, a k-ω formulation of a standard k-ε model is derived and merged together with the previous model via a blending function being one in the near wall region to activate the standard k-ω model and zero outside activating the k-ε model. In its standard formulation, the k-ω SST is also not sensitized to flow rotation and curvature.

The Reynolds Stress Model of Elena and Schiestel [5]

The approach presented by Poncet et *al.* [22, 23] is based on one-point statistical modeling using a low Reynolds number second-order full stress transport closure sensitized to rotation effects by Elena and Schiestel [5]. This approach allows for a detailed description of near-wall turbulence and is free from any eddy viscosity hypothesis. Four terms compared to the former model of Launder and Tselepidakis [14] have been added in this version. They account for the implicit effects of rotation on turbulence and act only when the flow is subjected to strong rotation. $\Phi_{ij}^{(R)}$ is a part of the pressure-strain correlation term sensitized to the dimensionality tensor C_{ij}. The modeling of its linear effect is deduced from the spectral tensor modeling of Schiestel and Elena [24]. D_{ij}^{R} is an inhomogeneous diffusion term, which slows down the tendency to bidimensionalization for wall bounded flows. B_{ij} is a homogeneous source term, which rectifies the pressure-strain correlation and which acts only in case of strong rotation. It produces spectral phase scrambling (angular dispersion). The rotation also reduces the energy transfer from large to small turbulent scales. It is modeled through an inverse flux J_{ij} considered as isotropic for high Reynolds number. It is a correction term of the dissipation ε_{ij}, which increases the turbulence levels in the core of the flow. These four terms are defined as follows:

$$\Phi_{ij}^{(R)} = -0.6[(\mathcal{D}_{cij} + \frac{1}{2}\mathcal{D}_{c\Omega ij}) - \frac{2}{3}P_c\delta_{ij}] - \frac{2}{5}k(V_{i,j} + V_{j,i}) \quad (1)$$

$$D_{ij}^{R} = (c_s\frac{k^2}{\varepsilon}f_{Ro}Y_{lm}R_{ij,l})_{,m} \quad (2)$$

$$B_{ij} = -\alpha_B(R_{ij} - k\delta_{ij} + \frac{1}{2}C_{ij}) \quad (3)$$

$$J_{ij} = \frac{2}{3}[(1 - f_T)\delta_{ij} + f_T\frac{3R_{ij}}{2k}]J \quad (4)$$

The dissipation rate equation ε is the one proposed by Launder and Tselepidakis [14]. The turbulence kinetic energy equation, though it is redundant in a RSM model, is solved numerically in order to get faster convergence. The complete model is given in [5].

The Reynolds Stress Model has been implemented in a finite-volume code using staggered grids for mean velocity components with axisymmetry hypothesis in the mean and non staggered grids for the Reynolds stress tensor. The code is steady elliptic. The velocity-pressure coupling is solved using the SIMPLER algorithm. In order to overcome stability problems, several stabilizing techniques are introduced in the numerical procedure. Also, the stress component equations are solved using matrix block tridiagonal solution to enhance stability using nonstaggered grids.

ROTATING CAVITY WITH AN RADIAL OUTFLOW

A cavity formed between two co-rotating coaxial disks is a common feature in rotating machinery and, in particular, in gas turbine engine compressor and turbine rotor assem-

blies. This configuration is also well suited for meteorological studies of the Earth's lower atmosphere. The flow behaviour in such cavity is strongly dependent on whether there is a throughflow of fluid in the cavity and on the temperature between the walls. A radial outflow is sometimes injected within the whellspace to cool the hot surfaces of the disks. In the case of a radial outflow, the mean secondary flow in the cavity can be characterized by a rotating inviscid core and two disk boundary layers. The flow structure may be highly complex with the coexistence of laminar and turbulent flow regions and/or the presence of three-dimensional vortical structures embedded in a turbulent flow regime. For an uniform temperature distribution along the disks, Owen et *al*. [20] identified four flow regions within the cavity (Fig.1): a source region close to the inlet, two Ekman type layers along the disks, a sink region at the periphery and an interior core separating the Ekman layers. This arrangement is very challenging for turbulence modelings.

Geometrical configurations

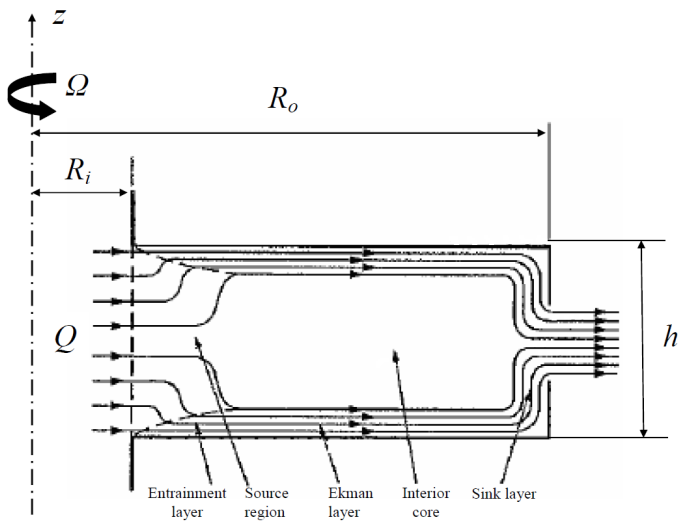

Figure 1: Schematic representation of the rotating cavity with an outward radial throughflow with characteristic streamline patterns, after Owen and Pincombe [19].

The cavity sketched in Figure 1 is composed of two smooth parallel disks of outer radius $R_o = 190$ mm and inner radius $R_i = 19$ mm separated by an axial gap $h = 50.73$ mm. All walls rotate at the same rotation rate Ω. A volume flow rate Q of air is supplied radially to the cavity through the entire disk gap h. The mean flow is mainly governed by four flow control parameters: the aspect ratio of the cavity L, its radius ratio s, the rotational Reynolds number Re based on the outer radius of the rotating disk R_o and the volume flow rate coefficient C_w.

$$L = \frac{R_o - R_i}{h} = 3.37 \qquad s = \frac{R_i}{R_o} = 0.1$$

$$Re = \frac{\Omega R_o^2}{\nu} = 10^5 \qquad C_w = \frac{Q}{\nu R_o} = 1092$$

where ν is the fluid kinematic viscosity. A modified Rossby number $\epsilon_r = \frac{Q}{4\pi r^2 \Omega \delta}$ is sometimes used to quantify the relative effect of the throughflow compared to the one of rotation, with $\delta = \sqrt{\nu/\Omega}$ the thickness of the Ekman layer over a single infinite rotating disk. We define also the following dimensionless quantities: the dimensionless radial $r^* = (r - R_i)/(R_o - R_i)$ and axial $z^* = z/h$ positions.

Computational details

Computations have been performed using the RSM of Elena and Schiestel [5] and two-equation models (standard $k-\epsilon$ and $k-\omega$ models and a $k-\omega$ SST model) combined with a low Reynolds number approach. These models are available within the commercial code Fluent 6.3. For all models, a 160×100 mesh in the (r, z) frame provides a grid independent solution for the configuration corresponding to the experiments of Owen and Pincombe [19]. It is also verified that the grid is sufficiently refined close the cylinders to describe accurately the viscous sublayers. The wall coordinate $z^+ = \Delta_1 z u^*/\nu$ (u^* the friction velocity at the wall and $\Delta_1 z/h = 0.0025$ the size of the first mesh in the radial direction) remains in the range $[0.5 - 1.6]$ along both disks. The size of the first mesh in the radial direction is $\Delta_1 r/h = 0.0054$. For the RSM, about 2000 iterations (2 hours) on the M2P2 cluster composed of 2 xeon quadcore 3 GHz are necessary to obtain the numerical convergence of the calculations. For the two-equation models, the convergence is reached after less than 1000 iterations (less than 1 hour) on a PC station.

The same initial and boundary conditions are imposed for all models. At the boundaries, all the variables are set to zero at the walls except for the tangential velocity, which is set to Ωr on rotating walls. At the inlet, an averaged radial velocity is imposed with a given low level of turbulence (3%). The mean tangential velocity is also fixed to the disk speed. At the outlet, several types of conditions have been tested. As no reversed flow has been observed in the experiments [19], the conservation of mass flow rate is imposed at the outlet. The calculations presented here are steady state adiabatic solutions.

Results

The axial profiles of the dimensionless tangential $V_\theta^* = V_\theta/(\Omega r)$ and radial V_r/V_{rm} velocity components are presented in figure 2a & c respectively at $r^* = 0.556$ for $Re = 10^5$ ($\epsilon_r = 0.423$). V_{rm} is the averaged radial velocity imposed at the inlet ($V_{rm} = Q/(2\pi R_i h)$). The predictions of the turbulence models are compared to the measurements of Owen and Pincombe [19] and also to the standard solutions for the Ekman layers (see in [19]):

$$V_r = -\bar{V_\theta} \exp(-z/\delta) \sin(z/\delta) \tag{5}$$

$$V_\theta = \bar{V_\theta}[1 - \exp(-z/\delta) \cos(z/\delta)] \tag{6}$$

with $\bar{V_\theta}$ given by Faller [7], who produced a power-series expansion of the non-linear terms of the Navier-Stokes equations for steady and laminar flow:

$$\bar{V_\theta} = \frac{-Q}{2\pi r \delta}(1 + 0.3\epsilon_r + 0.388\epsilon_r^2 \ldots) \tag{7}$$

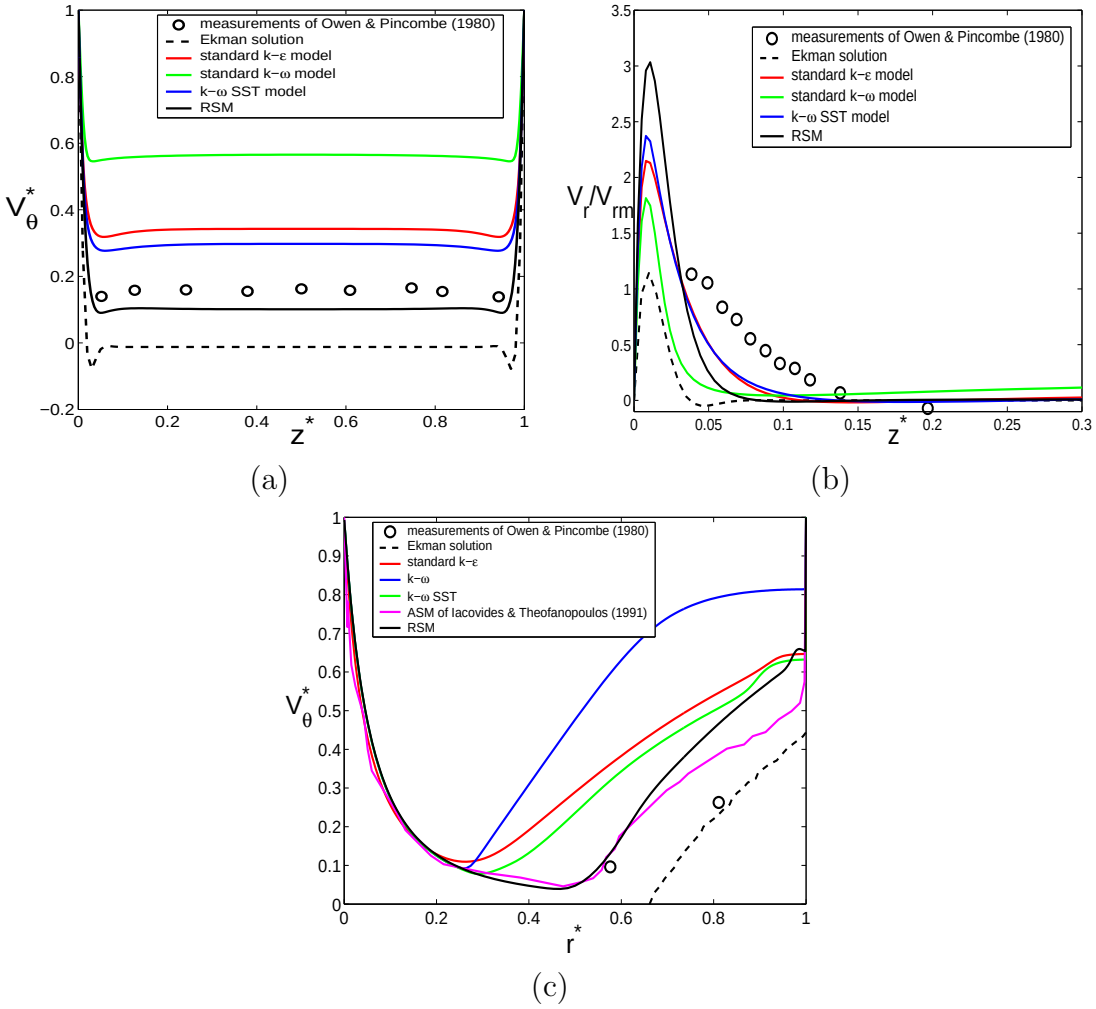

Figure 2: Axial distributions of the mean (a) tangential and (b) radial velocity profiles for $Re = 10^5$ ($\epsilon_r = 0.423$) at $r^* = 0.556$; (c) Radial distributions of the tangential velocity for the same parameters.

The flow is symmetrical about the mid-cavity plane, $z^* = 0.5$. Fluid entering the cavity at $r^* = 0$ is progressively entrained from the source region into the entraining boundary layers along the rotating walls. When all of the fluid is supplied by the source region has been entrained into the boundary layers, these boundary layers become non-entraining (see streamline patterns in figure 1). They are referred to as non-entrained

Ekman-type layers, by analogy with Ekman layers, where the magnitude of the relative tangential velocity of the fluid outside the layer is small in comparison with the disk speed: about 18% of the disk speed from the experiments and 12% from the RSM (Fig.2a). The two-equation models strongly overestimate the mean tangential velocity in the interior core. It is shown from the axial distribution of V_θ^* at $r^* = 0.556$ (Fig.2a) but also from the radial distributions (Fig.2c). The Ekman solution is not pertinent at $r^* = 0.556$ as it provides a negative value for V_θ^* in the core far from the measurements of Owen and Pincombe [19]. At the higher radii, the better agreement is obtained either using the RSM or with the Algebraic Stress Modeling (ASM) of Iacovides and Theofanopoulos [12]. In the outler region, the Ekman solution gets pertinent again, which indicates a relaminarization of the flow. The volume flow rate in each Ekman-type layers is $Q/2$ as no fluid flows outside the boundary layers from the RSM, which is not the case using the $k-\omega$ model (Fig.2b). There are no available measurements very close to the disks but it is clearly shown that all models fail to predict the thickness of the Ekman layer from the V_r profiles. The discrepancies may be explained by the appearance of three-dimensional instabilities either in the core or in the Ekman layers depending on the flow conditions [4]. These structures strongly affect the mean flow.

TAYLOR-COUETTE-POISEUILLE FLOWS

Test case 2 corresponds to a Taylor-Couette system subjected to an axial Poiseuille flow, which has been studied experimentally by Escudier and Gouldson [6] then numerically by Naser [17]. This kind of Taylor-Couette flows with a superimposed Poiseuille flow is of great importance, since these flows have many applications in process engineering (dynamic membrane filtration, rheology, UV disinfection, pasteurization), geophysics (mantle convection) and also in the turbomachinery industry for bearings, asynchronous motor with axial ventilation or rotating heat exchangers.

Geometrical configurations

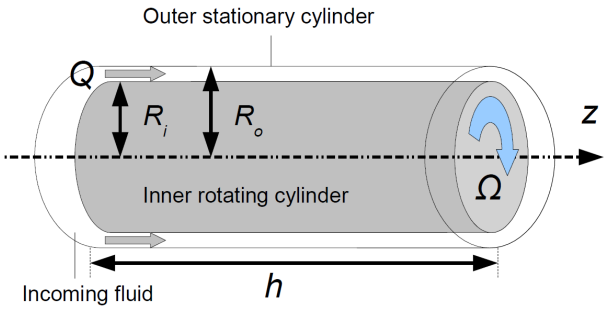

Figure 3: Schematic representation of the Taylor-Couette-Poiseuille configuration with relevant notations.

The cavity sketched in figure 3 is composed of two smooth concentric cylinders. The inner cylinder of radius R_i is rotating at a given rotation rate Ω, while the outer cylinder of radius R_o is stationary. This configuration is known in the litterature as the Taylor-Couette problem. The height of the cavity is denoted h in the following. An axial volume flow rate Q can be superimposed at the cavity inlet. The mean flow is mainly governed by four flow control parameters: the aspect ratio of the cavity L, its radius ratio s and the flow rate coefficient C_w already defined plus the Taylor number $Ta = \Omega R_i \Delta R/\nu$ based on the rotating speed of the inner cylinder ΩR_i and the hydraulic diameter $\Delta R = 2(R_o - R_i)$. The non dimensional parameter values considered here, that correspond to those related to the experiments performed by Escudier and Gouldson [6] under isothermal conditions are:

$$L = 0.0041 \qquad s = 0.506 \qquad Ta = 1922 \qquad C_w = 2839; 5914; 17742$$

where ν is the fluid kinematic viscosity. It corresponds to the experiments performed by Escudier and Gouldson [6] under isothermal conditions. The values of Ta considered here is much higher than the critical value $Ta = 420$ for the transition to turbulence found experimentally by Aoki et *al.* [1], which ensures that the flow is highly turbulent without Taylor vortices.

Computational details

Computations have been performed using the RSM of Elena and Schiestel [5] and two-equation models (standard $k-\epsilon$ and $k-\omega$ models and the $k-\omega$ SST) combined with a low Reynolds number approach. These models are the ones available within the commercial code Fluent 6.3. For all models, a 180×400 mesh in the (r, z) frame has been used. Thus, the wall coordinate $r^+ = \Delta_1 r u^*/\nu$ remains below 0.3 along both cylinders, which is quite below the classical value $r^+ = 1$. The sizes of the first mesh in the radial and axial directions are $\Delta_1 r/h = 5.65 \times 10^{-5}$ and $\Delta_1 z/h = 6.38 \times 10^{-3}$ respectively. About 30000 iterations (20 hours) on the M2P2 cluster composed of 2 xeon quadcore 3 GHz are necessary using the RSM to obtain the numerical convergence of the calculations. For the two-equation models, the convergence is reached after less than 10^3 iterations (less than one hour) on PC station.

All the variables are set to zero at the walls except for the tangential velocity V_θ, which is set to ΩR_i on the inner rotating cylinder and zero on the outer stationary cylinder. A linear profile for the mean tangential velocity component is imposed at the inlet. A parabolic profile is then imposed for the axial velocity V_z at the cavity inlet, with a given level of turbulence intensity (8%). At the outflow section, the pressure level is imposed, whereas the derivatives for all the other independent quantities are set to zero if the fluid leaves the cavity, and fixed external values are imposed if reversed flow occurs. It is noteworthy that reversed flows have never been observed in the present work, whatever the values of the flow control parameters. The calculations presented here are steady state adiabatic solutions.

Results

The predictions of the RSM and two-equation models are compared to the LDA measurements of Escudier and Gouldson [6] at a given axial position $z^* = z/h = 0.1$ for three values of the flow rate coefficient: $C_w = 2839$, 5914 and 17742. The mean tangential velocity component is normalized using the rotational speed of the inner cylinder ΩR_i, whereas the mean axial velocity component is normalized using the mean axial velocity $\overline{V_z}$ imposed at the inlet, defined by $\overline{V_z} = Q/(\pi(R_o^2 - R_i^2))$: $V_\theta^* = V_\theta/(\Omega R_i)$ and $V_z^* = V_z/\overline{V_z}$. To enable direct comparisons with the measurements, the tangential v'_θ and axial v'_z normal stresses are normalized by $\overline{V_z}$: $v_\theta^{'*} = \sqrt{\overline{v_\theta'^2}}/\overline{V_z}$ and $v_z^{'*} = \sqrt{\overline{v_z'^2}}/\overline{V_z}$.

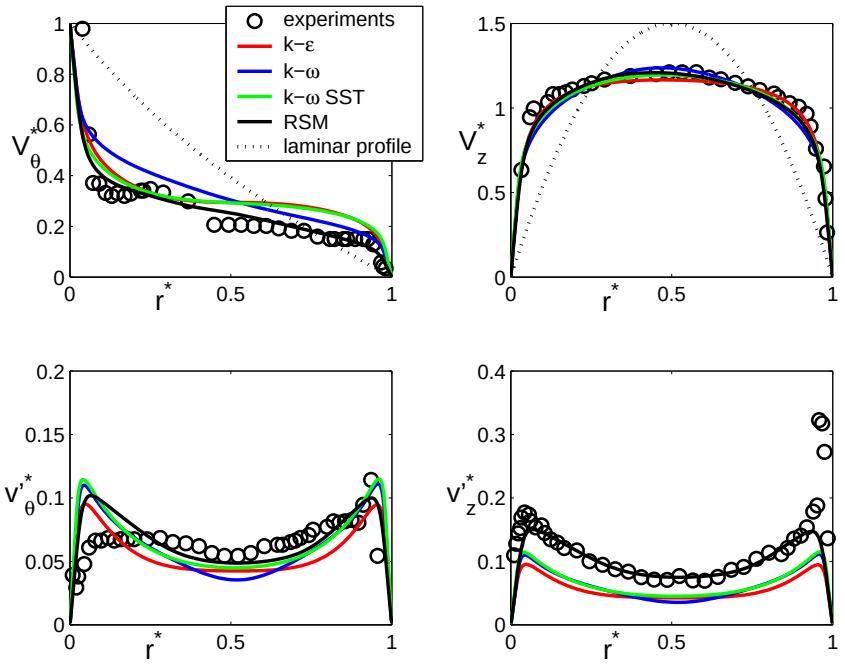

Figure 4: Radial distributions of the mean tangential and axial velocity components and of the tangential $v_\theta^{'*}$ and axial $v_z^{'*}$ normal Reynolds stress tensor components for $C_w = 17742$.

As it can be seen from Figure 4 for $C_w = 17742$, the predictions of all models are in good agreement with the experimental data for the mean axial velocity. The tangential velocity varies inversely with the radius from the measurements, which is well predicted by the RSM. At the same time, the $k - \epsilon$ and $k - \omega$ SST models predict a center body rotation. with a constant tangential velocity. The $k - \omega$ model predicts also the good trend but it overestimates V_θ^* outside the boundary layers with a relative error of 48%. All models offer a good description of the boundary layer thicknesses along the cylinders. It is noteworthy that the mean velocity profiles are far from the laminar ones highlighting the turbulent nature of the flow. Concerning the turbulent field, turbulence intensities are also relatively well predicted by the RSM, even if it does not reproduce the asymmetry of

the normal stress profiles observed in the experiment. The component $v_\theta^{'*}$ is overestimated by all models along the rotor, whereas they all underestimated the turbulence intensities along the stator. The two-equation models fail completely to reproduce the good levels for $v_z^{'*}$ in the whole gap.

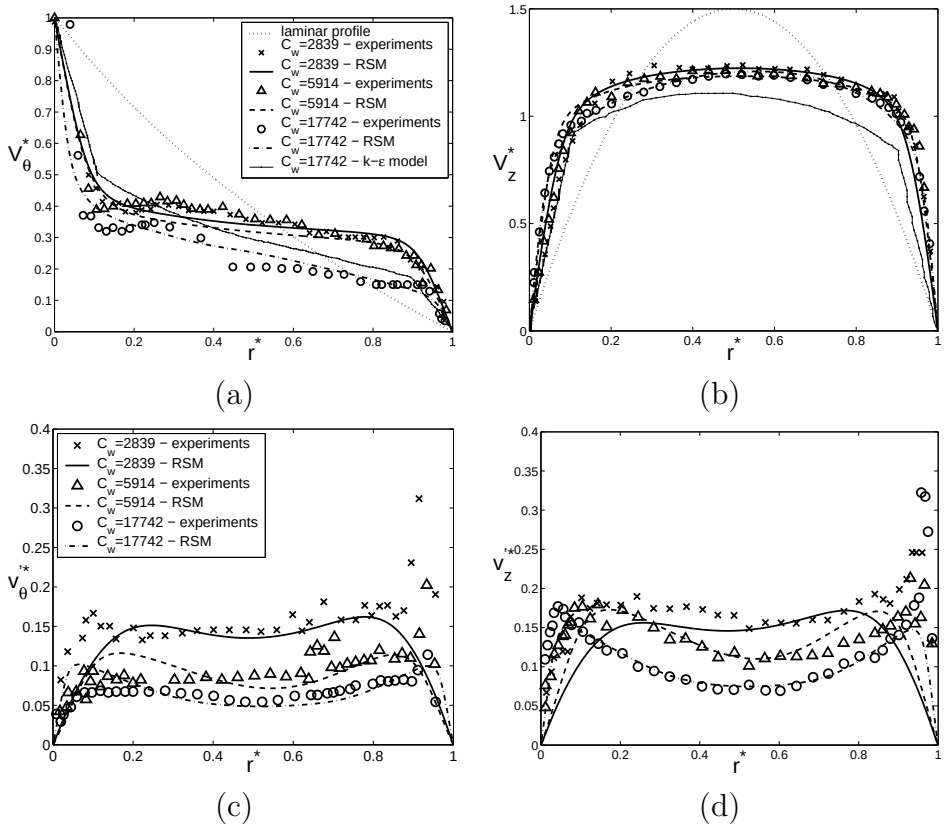

Figure 5: Radial distributions of the mean (a) tangential and (b) axial velocity components and of the (c) tangential $v_\theta^{'*}$ and (d) axial $v_z^{'*}$ normal Reynolds stress tensor components; Comparisons between the present RSM (lines) and the LDA measurements of Escudier and Gouldson [6] (symbols) for three values of C_w: $C_w = 2839$ ($\times$, $-$), $C_w = 5914$ ($\triangle$, $--$) and $C_w = 17742$ ($\circ$, $.-$). The laminar profiles (dotted lines) and the predictions of the $k-\varepsilon$ model of Naser [17] (dash-dotted) for $C_w = 17742$ are also shown.

Figure 5 shows the radial distributions of the dimensionless mean velocity components and the corresponding normal stresses at $z^* = 0.1$ for three values of the flow rate coefficient. For the two lowest values of C_w, the tangential velocity profiles (Fig.5a) exhibit a structure divided into three regions: two thin boundary layers developed on each cylinder separated by a core rotating at a constant velocity. The central region rotates at 32% (resp. 34%) of the cylinder speed for ($C_w = 2839$) (resp. ($C_w = 5914$)). The flow is here mainly governed by the rotation. An increase of the flow rate coefficient to $C_w = 17742$ implies a decrease of the rotating speed of the core region. Moreover, the tangential ve-

locity is no more constant in the gap but is inversely proportional to the radius. Thus, the mean angular momentum is almost constant in that region. There is only a weak effect of the flow rate coefficient on the radial distributions of the axial velocity (Fig.5b). The profiles are close to the turbulent Poiseuille flow profiles in pipes with a nearly constant axial velocity in the gap and thin boundary layers on the cylinders. For this value of radius ratio $s = 0.506$, the profiles are almost symmetric. The profiles become flatter with decreasing C_w as already noted by Nouri and Whitelaw [18]. It is noteworthy that, whatever the value of C_w, the mean velocity profiles are far from the laminar profiles highlighting the turbulent nature of the flow. For $C_w = 17742$, the RSM improves significantly the results of the $k - \varepsilon$ of Naser [17], which fails to predict the right profiles with large discrepancies for both the axial and tangential velocity components. The axial velocity is largely underestimated in the core and the tangential velocity is slightly overestimated. Fully developed conditions are reached at $z^* = 0.1$ using the RSM in agreement with the observations of Escudier and Gouldson [6], whereas the predictions of the $k - \varepsilon$ model of Naser [17] showed a large dependence of the tangential velocity profiles on the axial position. This last author attributed the discrepancies obtained by the $k - \varepsilon$ model to the fact that its model is blind to any rotation effects, and that the eddy viscosity concept, on which this model is based, is unsuitable with the present flow situation. On the contrary, the present RSM model is both sensitized to rotation effects [5] and free from any eddy viscosity hypothesis, which may explain the better overall agreement with the experimental data.

Figures 5c & d present the radial distributions of the tangential and axial normal Reynolds stress tensor components for the same sets of parameters. Turbulence is mainly concentrated in the core region and vanishes towards the walls. The tangential and axial velocity fluctuations show a progressive decrease with increasing flow rate coefficient in agreement with the experimental data of Escudier and Gouldson [6] and the LES results of Chung and Sung [3]. It is attributed by Escudier and Gouldson [6] to the vortical structures observed for low C_w values induced by the centerbody rotation. For high values of C_w, the radial penetration of the rotational influence is reduced and turbulent fluctuations are suppressed as if there were no solid body rotation. The profiles of $v_\theta^{'*}$ and $v_z^{'*}$ are asymmetric for the lowest flow rate ($C_w = 2839$) in agreement with [3], which can be attributed to the destabilizing effect of the centrifugal forces. All these phenomenons are well reproduced by the RSM, which predicts also quite good the turbulent intensities in the core of the flow. Some discrepancies are obtained in the boundary layers, especially for the peak values very close to the walls. The variations in the radial direction of the turbulent levels along each cylinder are also smoother than the experimental ones, which was also the case for the LES results of Chung and Sung [3] against the measurements of Nouri and Whitelaw [18].

ROTOR-STATOR FLOWS WITH THROUGHFLOW

Test case 3 corresponds to a rotor-stator cavity with a superimposed axial throughflow studied experimentally by Poncet et *al.* [22, 23]. These flows are encountered in many industrial devices such as cooling-air systems in gas turbine engines for example and have been the subject of intense researches during the last decades as they offer a relatively simple configuration to study the influence of rotation on turbulence.

Geometrical configurations

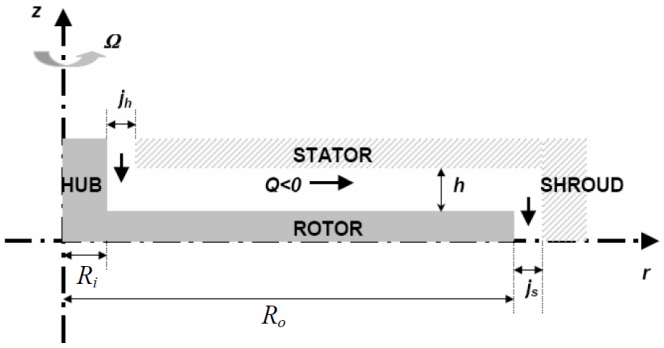

Figure 6: Schematic representation of the rotor cavity with an axial throughflow corresponding to the experiments of Poncet et *al.* [22, 23].

The cavity sketched in Figure 6 is composed of two smooth parallel disks of outer radius $R_o = 250$ mm and inner radius $R_i = 38$ mm separated by an axial gap h. The rotor and the hub attached to it rotate at the same rotation rate Ω, while the stator and the shroud are stationary. A centripetal or centrifugal volume flow rate Q of water can be supplied axially to the cavity through the two openings $j_h = 17$ mm and $j_s = 3$ mm. Different values of the physical parameters have been considered (see Table 1). Note that a negative (resp. positive) value of the flow rate coefficient C_w corresponds to a centrifugal (resp. centripetal) throughflow.

case	aspect ratio L	radius ratio s	Reynolds number Re	flowrate coefficient C_w
3-1	23.56	0.152	4.15×10^6	0
3-2	23.56	0.152	1.04×10^6	9881
3-3	70.67	0.152	1.04×10^6	-5159

Table 1: Values of the flow control parameters for the three cases in the rotor-stator configuration.

Computational details

All calculations using the two-equation models were performed with the commercial CFD 3D solver CFX-12.0. As there is no evidence of three-dimensional structures embedded in the turbulent flow, the numerical domains consist in a 5° sector. A mesh independence analysis was done and a 300×140 mesh in the (r,z) frame proved to be sufficient for the low Reynolds calculations while a 240×70 mesh in the (r,z) frame was selected for the high Reynolds one. The calculations presented here are steady state adiabatic solutions. Referring to the near wall treatment, low and high Reynolds number approaches are used in conjunction with the SST model, while wall functions are selected for the $k-\epsilon$ model coherently with the solver limitations.

For the RSM, a 140×80 mesh in the (r,z) frame proved to be sufficient in cases 3-2 and 3-3 in the present work to get grid-independent solutions. The wall coordinate z^+ remains below 0.2 along both disks in that cases. The sizes of the first mesh in the radial and axial directions are $\Delta_1 r/h = 5.47 \times 10^{-3}$ and $\Delta_1 z/h = 1.529 \times 10^{-4}$ respectively. It has been verified that the numerical solution is, indeed, accurate within 1.5% (maximum error for velocity and stress components) compared to the solution obtained on a mesh using twice the number of nodes. Nevertheless, a more refined mesh 200×100 is necessary for the case 3-1 where a higher Reynolds number is computed. About 20000 iterations (10 hours on the NEC SX-5 from the IDRIS center in Orsay) were necessary to obtain the numerical convergence of the calculation. All the variables are set to zero at the walls except for the tangential velocity V_θ, which is set to ΩR_i on the rotor. At the inlet, a linear profile for the mean tangential velocity and a parabolic profile for the axial velocity V_z are imposed together with a given low turbulence level of 1%. In the outflow section, the pressure is permanently fixed, whereas the derivatives for all the other independent quantities are set to zero if the fluid leaves the cavity, and fixed external values are imposed if reversed flow occurs, which may be the case under certain conditions of flow rate.

Results

We first consider the turbulent flow $Re = 4.15 \times 10^6$ in a closed rotor-stator system of aspect ratio $L = 23.56$ with no throughflow (case 3-1). The turbulence models are compared to the LDA and pressure measurements of Poncet et *al.* [22]. For this set of parameters, the flow clearly exhibits a Batchelor structure at mid-cavity $r^* = 0.48$ (Fig.7): two boundary layers, one on each disk, separated by a central inviscid core in solid body rotation. The core is characterized by a zero radial velocity, which ensures that there is no viscous shear stress and by a constant tangential one. The Bödewadt layer along the stator is centripetal and, by conservation of mass, the Ekman layer along the rotor is centrifugal. The tangential velocity in the core is equal to 45% of the disk speed, which is characteristic of the turbulent regime. The thickness of the Bödewadt layer as well as the extremum value reached by the radial velocity in that boundary layer are better predicted by the RSM compared to the two-equation models. An overall good agreement

is obtained between the experimental data and the model predictions for the mean field. Regarding the turbulent field, turbulence is confined in the boundary layers, whereas the core remains almost laminar. The levels of the two normal components of the Reynolds stress tensor are quite similar with intensities slightly higher along the rotor side from the numerical profiles. The RSM predicts quite well the normal stresses along the rotor. Along the stator, all turbulence models underestimate the turbulence intensities. From the RSM, the cross-component $R^*_{r\theta}$ is almost zero in the core in agreement with the LDA data. Thus, there is no turbulent shear stress in that region. The other cross components, not shown here, are also negligible in the core, which means that the gradients $\partial V_\theta/\partial z$ and $\partial V_\theta/\partial r$ are weak. It confirms the existence of an inviscid core in solid body rotation. It shows also that the turbulence production is almost zero in that region and so that turbulence is only due to the diffusion phenomenon.

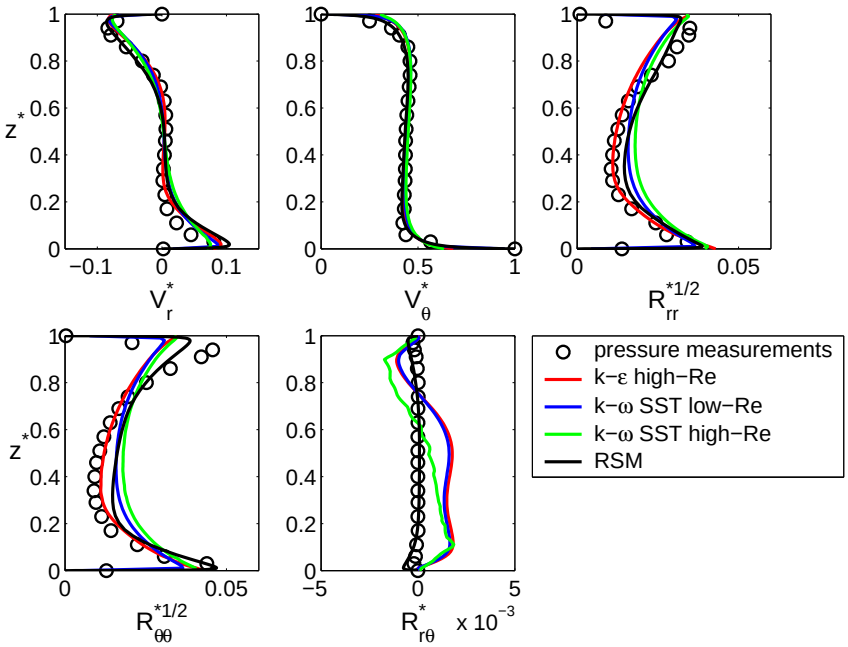

Figure 7: Axial profiles of the mean radial and tangential velocity components and the corresponding Reynolds stress tensor components at $r^* = 0.48$ for $L = 23.89$, $Re = 4.15 \times 10^6$ and $C_w = 0$.

An axial inflow is now supplied to the cavity (Case 3-2). In that case, one interesting phenomenon is that the central core observed in the previous case without throughflow can rotate faster than the rotor under certain conditions of rotation and imposed flow rate. For the set of parameters considered here ($Re = 1.04 \times 10^6$, $C_w = 9881$), the inviscid core is still observed but at $r^* = 0.48$, it rotates at the same angular velocity than the rotor. As shown by Poncet et *al.* [22], the flow preserves the Batchelor flow structure for $r^* \geq 0.48$, whereas the core can rotate up to three times faster than the disk at the inner radii. The imposed inflow is here strong enough to suppress the outflow

along the rotor due to the centrifugal force. Thus, the radial velocity is negative whatever z^*. All models underestimate the mean tangential velocity in the core, which may be attributed to different prerotation levels imposed at the inlet between the experiment and the calculations. Its value is fixed to half the maximum disk speed in the turbulence models, whereas it slightly varies between 0.5 and 0.55 in the experiments depending on C_w [21]. Turbulence is mainly confined in the Bödewadt layer along the stator. The turbulent field is very well predicted by the RSM, while the other models underestimate the turbulence intensities essentially in the core and along the stationary disk. The shear stress $R^*_{r\theta}$ is well computed using the RSM even if the values are quite weak.

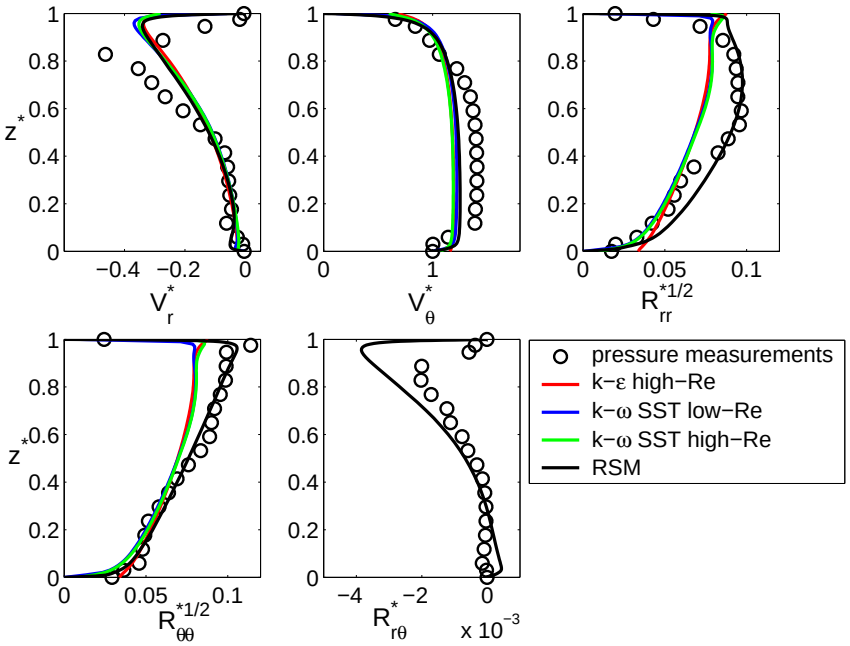

Figure 8: Axial profiles of the mean radial and tangential velocity components and the corresponding Reynolds stress tensor components at $r^* = 0.48$ for $L = 23.89$, $Re = 1.04 \times 10^6$ and $C_w = 9881$.

One interesting feature in rotor-stator flows is the transition from the Batchelor flow structure already observed in cases 3-1 and 3-2 to the one proposed by Stewartson [25]. This last author showed indeed that the tangential velocity is almost zero between the disks apart from a thin boundary layer along the rotor. The controversy between Batchelor and Stewartson came to end in 1983 when Kreiss and Partner [13] studied the existence and uniqueness of solutions for a two infinite disk configuration. They showed the existence of a class of multiple solutions depending on the initial conditions. In finite rotor-stator disk systems, the Stewartson flow structure has been observed essentially when an axial or radial outflow is superimposed to the main tangential flow. Figure 9 displays the velocity profiles corresponding to the case 3-3 considered experimentally by Poncet et *al.* [23] for different radial positions. Note that no experimental data for the turbulent field

are available in this case. For the mean field, depending on the radial location, the flow belongs either to the Batchelor flow regime or to the Stewartson one. Regarding the radial velocity profiles, the flow is centrifugal in the whole cavity for this set of parameters. For $r^* = 0.34$, the flow is a Stewartson-type flow with only one boundary layer on the rotor. The core disappeared ($V_\theta^* \simeq 0.05$ at $z^* = 0.5$) and the radial velocity becomes significant compared to the tangential velocity. The mean radial velocity profile is besides close to a Poiseuille-like profile in pipes. For $r^* = 0.62$, the flow switches continously to Batchelor type with two separated boundary layers when one regards the tangential velocity profile. The central core reappears as V_θ^* has increased to 0.11 from the measurements (0.16 from the turbulence models). When one moves closer to the periphery ($r^* = 0.91$), the tangential velocity at mid-height increases up to 0.23 from the experimental profile (0.29 from the turbulence models). The radial velocity distribution becomes asymmetric at this position. Even if the flow is outward along the stationary disk, the radial velocity is greater along the rotor due to the combined effect of the centrifugal force due to rotation and to the imposed outflow. All turbulence models selected here provide similar results. Even if high Reynolds approaches do not describe accurately the boundary layers, all models predict quite well the transition from one structure to another. Even if the values are quite weak, the pressure distribution (not shown here), which is a sensitive quantity for turbulence models, is also quite well predicted. In the present case, the main failure arises from the LDA technique used by Poncet et *al.* [23]. When the interdisk space is small ($L = 70.67$, $h = 3$ mm), as compared to the probe volume of the anemometer in the axial direction (0.8 mm), the measurements failed indeed. The integration of the mean radial velocity profile calculated by the turbulence models is in agreement with the imposed centrifugal throughflow rate, whereas it is not the case for the experimental data. The experimental values underestimate the radial and tangential velocities because these are integrated values on a too big probe volume compared to the interdisk space.

CONCLUSIONS

Turbulence modelings of three turbulent rotating flow arrangements have been performed using both the second-order closure of Elena & Schiestel [5] sensitized to rotation effects and two-equation models available within commercial CFD codes. Their predictions have been compared to experimental data available in the literature.

In the case of a rotating cavity with a radial outflow, all models fail to predict the right mean velocity profiles with large discrepancies for the tangential velocity in the core and the Ekman layer thicknesses compared to the measurements of Owen and Pincombe [19]. The best agreement for the tangential velocity distribution is obtained using the RSM. The difficulty arises in fact from the boundary conditions at the outlet, where imposing the mass flow rate is the only way to stabilize the calculation. It may be explained that the appearance of three-dimensional instabilities in the Ekman layers, which strongly affects the mean flow [4]. Thus, three-dimensional RANS calculations are then required.

Some comparisons have then been performed in a very elongated Taylor-Couette sys-

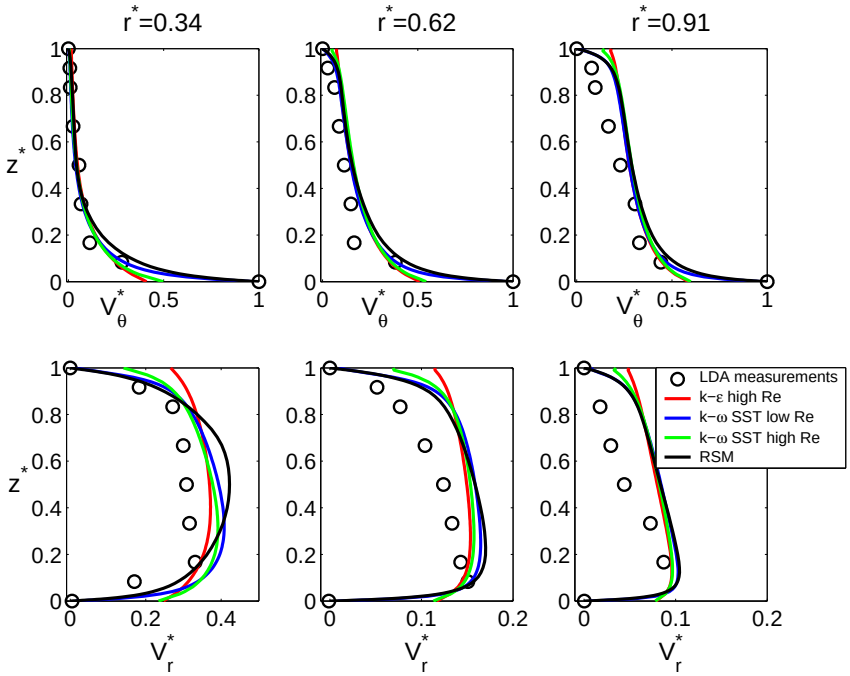

Figure 9: Axial profiles of the mean radial and tangential velocity components at three radial positions for $L = 70.67$, $Re = 1.04 \times 10^6$ and $C_w = -5159$. Comparisons between LDA measurements ($\circ$), the k-ε model high Re (red line), the k-ω SST low Re (blue line), the k-ω SST high Re (green line) and the RSM (black line).

tem with an imposed axial Poiseuille flow. The effect of the flow rate on the hydrodynamic field has been investigated. For all sets of parameters, the RSM has been very favorably compared to the velocity measurements of Escudier and Gouldson [6]. In particular, it improves significantly the predictions of the $k-\epsilon$ model of Naser [17] for the mean velocity distributions. Even if the RSM does not predict the asymmetry of the fluctuating velocity profiles, the computed turbulence intensities in the core region are in good agreement with the experimental data. All models predict quite well the mean field but the two-equation models completely fail to predict the turbulent quantities both in the boundary layers and in the core.

Finally, some computations have been done in a rotor-stator cavity corresponding to the experimental test rig of Poncet [21, 22, 23]. Whatever the flow configuration (with or without an axial inward or outward throughflow), all models, including either a low- or high- Reynolds number approach, provide very satisfactory results for both the mean and turbulent fields. The value of the tangential velocity in the core region and the extremum values of the radial velocity and the normal stresses along both disks are well captured even by the two-equation models. The transition to a core rotating faster than the disk due to the inward throughflow as well as the transition between the Batchelor and Stewartson flow structures when an outflow is enforced, are catched by all models. For

industrial applications, the $k-\omega$ SST model seems to offer a good compromise between accuracy and calculation cost.

REFERENCES

[1] H. Aoki, H. Nohira and H. Arai, Convective heat transfer in an annulus with an inner rotating cylinder, *Bulletin of JSME*, **10** (39), 523–532 (1967).

[2] J. B. Cazalbou, P. Chassaing, G. Dufour and X. Carbonneau, Two-equation modeling of turbulent rotating flows, *Phys. Fluids*, **17**, 055110 (2005).

[3] S. Y. Chung and H. J. Sung, Large-eddy simulation of turbulent flow in a concentric annulus with rotation of an inner cylinder, *Int. J. Heat Fluid Flow*, **26**, 191–203 (2005).

[4] E. Crespo del Arco, P. Maubert, A. Randriamampianina and P. Bontoux, Spatio-temporal behaviour in a rotating annulus with a source-sink flow, *J. Fluid Mech.*, **328**, 271–296 (1996).

[5] L. Elena and R. Schiestel, Turbulence modeling of rotating confined flows, *Int. J. Heat and Fluid Flow*, **17**, 283–289 (1996).

[6] M. P. Escudier and I. W. Gouldson, Concentric annular flow with centerbody rotation of a Newtonian and a shear-thinning liquid, *Int. J. Heat Fluid Flow*, **16**, 156–162 (1995).

[7] A. J. Faller, An experimental study of the instability of the laminar Ekman boundary layer, *J. Fluid Mech.*, **15**, 560–576 (1963).

[8] T. B. Gatski and C. G. Speziale, On explicit algebraic stress models for complex turbulent flows, *J. Fluid Mech.*, **254**, 59–78 (1993).

[9] A. Hellsten, Some improvements in $k-\omega$ SST turbulence model, *AIAA paper* 98-2554, 29th AIAA fluid Dynamics Conference, Albuquerque (1998).

[10] J. H. G. Howard, S. V. Patankar and R. M. Bordynuik, Flow prediction in rotating ducts using Coriolis-modified turbulence models, *J. Fluids Eng.*, **102**, 456–461 (1980).

[11] G. Iaccarino, A. Ooi, B. A. Petterson Reif and P. Durbin, RANS simulations of rotating flows, *Annual Research Briefs*, Center for Turbulence Research (1999).

[12] H. Iacovides and I. P. Theofanopoulos, Turbulence modeling of axisymmetric flow inside rotating cavities, *Int. J. Heat Fluid Flow*, **12 (1)**, 2–11 (1991).

[13] H.O. Kreiss and S.V. Parter. On the swirling ow between rotating coaxial disks : existence and uniqueness. *Commun. Pure Appl.Math.*, **36**, 55–84 (1983).

[14] B. E. Launder and D. P. Tselepidakis, Application of a new second moment closure to turbulent channel flow rotating in orthogonal mode, *Int. J. Heat Fluid Flow*, **15 (1)**, 2–10 (1994).

[15] C. A. Long and J. M. Owen, The effect of inlet conditions on heat transfer in a rotating cavity with a radial outflow of fluid, *J. Turbomachinery*, **108**, 145–152 (1986).

[16] F. R. Menter, Two-equation eddy viscosity turbulence models for engineering applications, *AIAA Journal*, **32**, 1598–1605 (1994).

[17] J. A. Naser, Prediction of Newtonian and Non-Newtonian flow through concentric annulus with centerbody rotation, *Int. Conf. on CFS in Mineral and Metal Processing and Power Generation*, CSIRO (1997).

[18] J. M. Nouri and J. H. Whitelaw, Flow of Newtonian and Non-Newtonian Fluids in a Concentric Annulus With Rotation of the Inner Cylinder, *J. Fluid Eng.*, **116**, 821–827 (1994).

[19] J. M. Owen and J. R. Pincombe, Velocity measurements inside a rotating cylindrical cavity with a radial outflow of fluid, *J. Fluid Mech.*, **99 (1)**, 111–127 (1980).

[20] J. M. Owen, J. R. Pincombe and R. H. Rogers, Source-sink flow inside a rotating cylindrical cavity, *J. Fluid Mech.*, **155**, 233–265 (1985).

[21] S. Poncet, Écoulements de type rotor-stator soumis à un flux axial: de Batchelor à Stewartson, *PhD thesis, Université de Provence*, (2005).

[22] S. Poncet, M. P. Chauve and R. Schiestel, Batchelor versus Stewartson flow structures in a rotor-stator cavity with throughflow, *Phys. Fluids*, **17**, 075110 (2005).

[23] S. Poncet, R. Schiestel and M. P. Chauve, Centrifugal Flow in a Rotor-Stator Cavity, *J. Fluid Eng.*, **127**, 787–794 (2005).

[24] R. Schiestel and L. Elena, Modeling of Anisotropic Turbulence in Rapid Rotation, *Aerospace Science and Technology*, **7**, 441–451 (1997).

[25] K. Stewartson. On the flow between two rotating coaxial disks, *Proc. Camb. Phil. Soc.*, **49**, 333–341 (1953).

[26] M. Wilson, J. X. Chen and J. M. Owen, Computation of flow and heat transfer in rotating-disc systems, *IMechE*, 41–49 (1996).